Journal of Bio- and Tribo-Corrosion (2022) 8:106
https://doi.org/10.1007/s40735-022-00706-9

# Investigation of Corrosion Characteristics of Plasma-Sprayed Composite Coating on Bearing Steel Through Electrochemical and Salt Spray Test

K Mohammed Ibrahim[1] · Sourabha S Havaldar[2] · Adarsha Hiriyannaiah[3] · R. Keshavamurthy[4]

Received: 3 June 2022 / Revised: 29 August 2022 / Accepted: 8 September 2022 / Published online: 21 September 2022


**Abstract**

This paper evaluates corrosion characteristics of a new material combination for a composite coating consisting of compounds Nickel Aluminum (NiAl), Aluminum oxide ($Al_2O_3$), and Cerium Oxide ($CeO_2$). Composite coating $NiAl + Al_2O_3 + CeO_2$ in the ratio of $70 + 10 + 20$ is sprayed on EN31 through atmospheric plasma spray (APS) technique. Scanning electron microscopy/energy-dispersive analysis (SEM/EDAX), X-ray diffraction (XRD), and optical microscopy (OM) were used to characterize microstructure of the coating, porosity, and coating thickness. Potentiodynamic test followed by electrochemical impedance spectroscopy (EIS) data analysis and salt spray test were performed to evaluate corrosion characteristics. Area % porosity for $NiAl + Al_2O_3 + CeO_2$ composite coating was found to be 1.34%. Coated EN31 shows 27% higher corrosion resistance compared to uncoated EN31 in Tafel plot and has a corrosion potential (Ecorr) of − 0.53 V which is 30% more when compared with uncoated EN31 under electrochemical test. Uncoated EN31 lost 5 times more weight than the coated EN31 under salt spray test conducted in a neutral mist of 5 wt% Sodium Chloride (NaCl) at 35 °C for 48 h. Under both the tests, results indicated that the composite coating $NiAl + Al_2O_3 + CeO_2$ on EN31 exhibits better corrosion resistance on account of protective oxide layer formed on the surface when compared with the uncoated EN31.

**Keywords** Tafel plot · Electrochemical impedance spectroscopy · Salt spray test

## 1 Introduction

Bearings operating in extreme environments are subjected to contamination that includes dirt, dust, and abrasive grit. These foreign particles get into bearing lubricants causing wear, corrosion, and resulting in premature bearing failure [1]. The abbreviations used in the paper are listed in Table 1. Different types of coating system based on Ni graphite were developed and corrosion resistance of the developed coating systems was studied using salt spray and electrochemical test. NaCl neutral solutions at 35 °C was used in polarization test and investigation concluded that the coating system having 96NiCr-4Al bond coat exhibited better corrosion resistance [2]. Plasma-sprayed NiCrAlY/mullite-coated high silicon cast iron alloy were subjected to EIS analysis and it was found that coating showed high resistance to corrosion [3]. Corrosion characteristics of two different coating systems were evaluated and it was concluded that CoNiCrAlY coating had 1.6 times higher corrosion density in Tafel analysis [4]. EIS and polarization test on NiTi intermetallic coatings indicate that the corrosion resistance is better when coated through HVOF than APS coating [5].YSZ-coated 304 stainless steel showed enhanced corrosion resistance than uncoated counterpart when subjected to EIS and polarization test [6].HVOF-coated ceramic composite $Cr_3C_2$–25%NiCr samples exhibited high resistance to corrosion than the plasma-sprayed coupons in polarization and EIS tests [7].Carbon steel surface plasma sprayed with 8YSZ immersed in seawater showed better corrosion in EIS test evaluation [8]. Low carbon steel was coated with different compounds such as $ZrO_2$, $Al_2O_3$, and $ZrO_2$/$Al_2O_3$ using APS technique. $Al_2O_3$/$ZrO_2$ coating has high corrosion resistance under polarization test, salt spray test,

✉ K Mohammed Ibrahim
mohammedkmails@gmail.com

[1] VTU-RRC, Bangalore 560078, Karnataka, India

[2] R.V. College of Engineering, Bangalore 560059, Karnataka, India

[3] Jain University, Bangalore 560069, Karnataka, India

[4] Dayananda Sagar College of Engineering, Bangalore 560078, Karnataka, India

**Table 1** Table of abbreviations

| NiAl | Nickel aluminum |
|---|---|
| $Al_2O_3$ | Aluminum oxide |
| $CeO_2$ | Cerium oxide |
| SEM | Scanning electron microscopy |
| EDAX | Energy-dispersive analysis |
| APS | Atmospheric plasma spray |
| XRD | X-ray diffraction |
| EIS | Electrochemical impedance spectroscopy |
| NaCl | Sodium chloride |

and immersion test [9]. $Cr_2O_3$ coating offers high resistance to corrosion resistance when compared with uncoated steel substrates under salt spray test for various time periods in 5% NaCl solution as per ASTM B117 standard [10]. Amorphous/nanocrystalline coatings showed better corrosion resistance in a NaCl corrosion medium used in electrochemical test [11]. AZ91 substrate coated with NiAl10 and NiAl40 coatings using APS and it was observed that coatings had improved corrosion resistance properties [12]. NiAl has excellent oxidation resistance, good thermal conductivity, with low density, and has melting point of 1638 °C and is an intermetallic compound [13]. Plasma-sprayed NiAl coatings have high porosity and it is found to be more than 5% [14]. Increased erosion resistance for NiCrSiB/$Al_2O_3$ coating was found due to low porosity of $Al_2O_3$ [15]. Composite coating $Al_2O_3$–Al showed better wear and corrosion resistance when compared with other traditional coatings [16]. Adding $CeO_2$ to the tungsten carbide-based coating improves coating hardness of the coating and significantly improves wear resistance of the coating [17, 18]. Although these compounds exhibit moderate tribological properties individually, there is very limited information available as regards to tribological properties of NiAl-$Al_2O_3$–$CeO_2$ composite coating on bearing steel EN31. Present investigation evaluates corrosion characteristics of a new material combination for a composite coating consisting of NiAl, $Al_2O_3$, and $CeO_2$. Composite coating NiAl + $Al_2O_3$ + $CeO_2$ in the ratio of 70 + 10 + 20 is sprayed on EN31 through atmospheric plasma spray (APS) technique [19]. As part of the investigation, microstructure of the coating, porosity, and coating thickness are studied along with evaluating corrosion characteristics of composite coating on EN31 by studying corrosion rate and weight loss under corroding environment for further experimental studies.

### 1.1 Sample Preparation

Bearing steel EN31 having rectangular shape with dimension 25 × 25 mm is used as substrate. Standard JIS1253-2013 was followed for optical emission spectrometry to identify chemical composition in EN31 and it is indicated in Table 2. Standard ASTM E10-18 was followed to determine the Brinell hardness and it was found to be 231. EN31 substrate surface was cleaned by utilizing sand blasting technique using 32 mesh size sand granules, and samples were correctly marked for clear identification.

### 1.2 XRD Analysis of Powder Feedstock

Elemental composition was determined for compounds NiAl, $Al_2O_3$, and $CeO_2$ by penetrating X-rays from XRD machine at angles between 0° and 90° on feedstock powders. XRD spectrum for NiAl is shown in Fig. 1a and it can be seen that the peak shape is sharp for Ni when compared with Al. XRD spectrum for $Al_2O_3$ is shown in Fig. 1b, and it is reflected with sharp peak shape. XRD pattern for $CeO_2$ is shown in Fig. 1c and has many sharp and short peaks indicating abundance of $CeO_2$.

### 1.3 Morphology of Powder Feedstock

Feedstock powders namely NiAl and $Al_2O_3$ were acquired from Spraymet Surface Technologies Pvt. Ltd and $CeO_2$ from Ritej Chemicals, India. Feedstock powder particle morphology investigations on NiAl, $Al_2O_3$, and $CeO_2$ were completed using SEM and EDAX. Particle size information was obtained through visual measurement using high-resolution SEM images. Figure 2a reveals NiAl powder particle in which Ni surface is masked with tiny Al particles and Fig. 2b shows energy spectrum for NiAl. EDAX analysis on NiAl powder showed Al particles having high weight percentage when compared with Ni particles as indicated in Table 3. Average particle size of NiAl is 3 µm and has spherical shape. Figure 3a shows $Al_2O_3$ powder particles having an average size of 10 µm with irregular shape, and Fig. 3b shows energy spectrum for $Al_2O_3$. Maximum weight percentage of oxygen was observed in $Al_2O_3$ compound as shown in Table 4. Figure 4a shows $CeO_2$ powder particle having an average size of 8 µm and particle with flake shaped, and Fig. 4b shows energy spectrum for $CeO_2$.

**Table 2** Chemical constituents of EN31

| Composition in % | | | | | | | |
|---|---|---|---|---|---|---|---|
| C | Mn | Si | P | S | Cr | Ni | Mo |
| 0.92 | 0.58 | 0.23 | 0.04 | 0.05 | 1.32 | 0.08 | 0.02 |

**Fig. 1** XRD spectrum for compounds **a** NiAl **b** $Al_2O_3$ **c** $CeO_2$

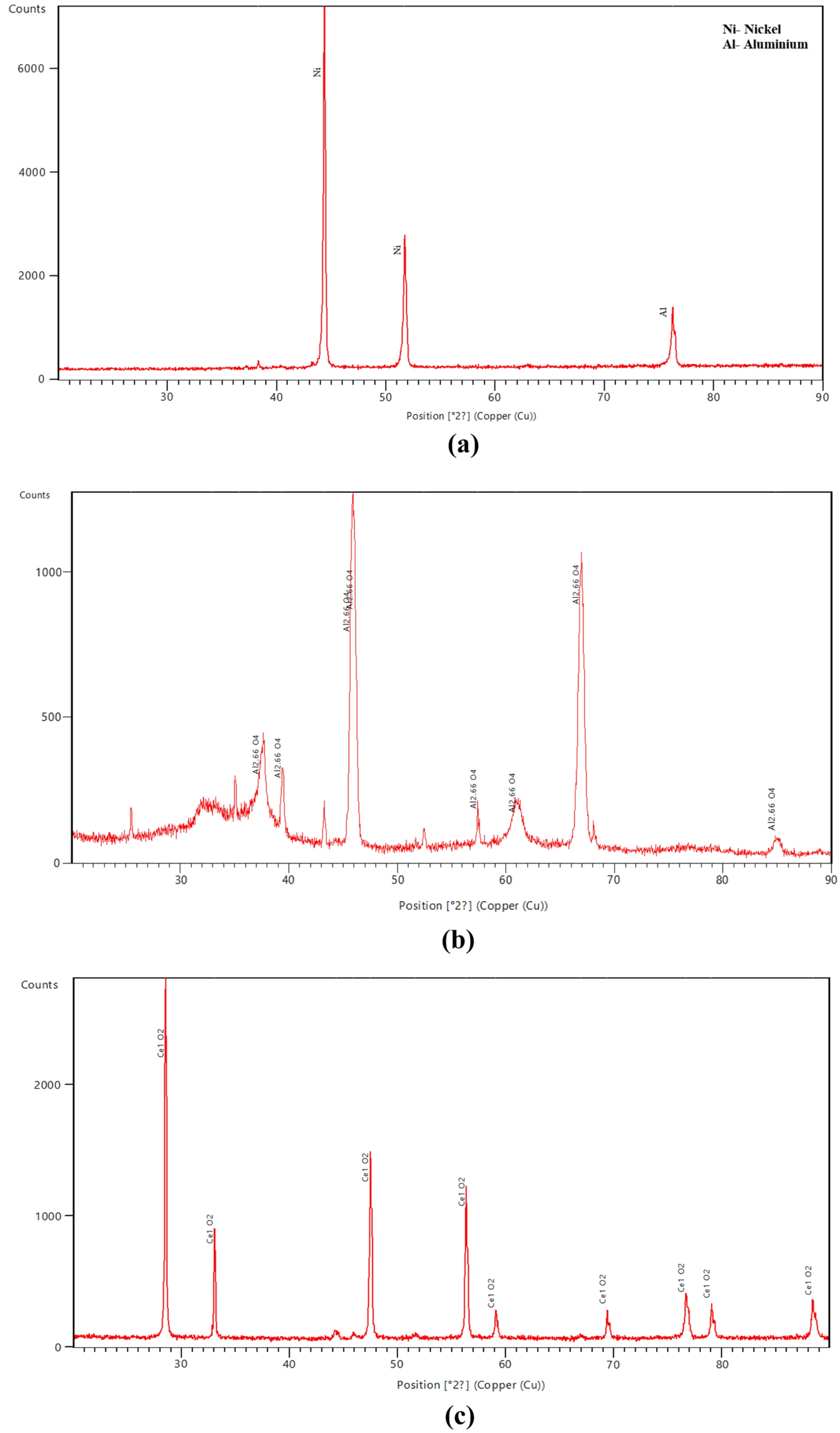

Fig. 2 EDAX analysis of powder feedstock NiAl (**a**) NiAl (**b**) Spectrum

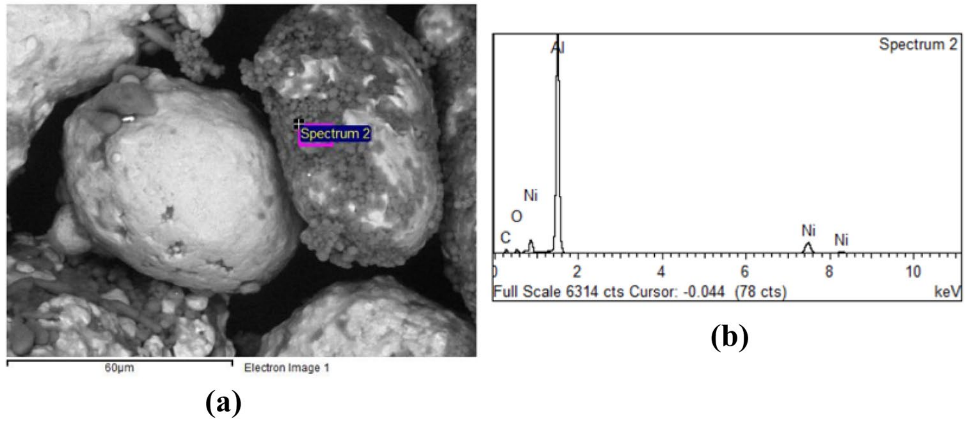


Table 3 EDAX analysis of NiAl

| Element line | Weight % |
|---|---|
| Al K | 68.20 |
| Ni K | 31.80 |
| Total | 100 |

Maximum weight percentage of Cerium was observed in $CeO_2$ compound as shown in Table 5.

## 1.4 Air Plasma Spray

$NiAl + Al_2O_3 + CeO_2$ powder composition mixture having a ratio of 70 + 10 + 20 was produced by utilizing ball milling technique and used as composite coating and sprayed on EN31 using APS technique with GH nozzle and 3 MB gun. Table 6 shows top coat and bond coat thickness, and Fig. 5 shows cross-sectional image of the coated EN31. Process parameters of APS for coating top and bond coat are indicated in Table 7. Coatings were performed at Spraymet Surface Technologies Pvt. Ltd. Bangalore, India.

Table 4 EDAX analysis of $Al_2O_3$

| Element line | Weight % |
|---|---|
| O K | 59.60 |
| Al K | 40.40 |
| Total | 100 |

## 1.5 Testing and Characterization

Optical Metallurgical Microscope (Zeiss—Axio Vert.A1) and Clemex Vision Image Analysis software (P.E. 7.0) equipment were used to measure porosity as per ASTM E2109-01 (RA2014) and Test Method B (Image Analysis). Nature of test was Area % Porosity by Image Analysis Method. Sample was cut into 3 × 3 mm and cross section was polished by building acrylic mold. Tests was repeated at ten different locations on cross section of each sample and average % porosity was computed. Electrochemical test and salt spray test were conducted on uncoated EN31 and $NiAl + Al_2O_3 + CeO_2$ coated EN31. Electrochemical test was conducted in standard three electrode cell, working electrode is an EN31 with exposed area of 1 $cm^2$ and is attached to Teflon holder using epoxy resin, counter electrode is a platinum foil having an area of 1 $cm^2$ and saturated calomel

Fig. 3 EDAX analysis of powder feedstock $Al_2O_3$ (**a**) $Al_2O_3$ (**c**) Spectrum

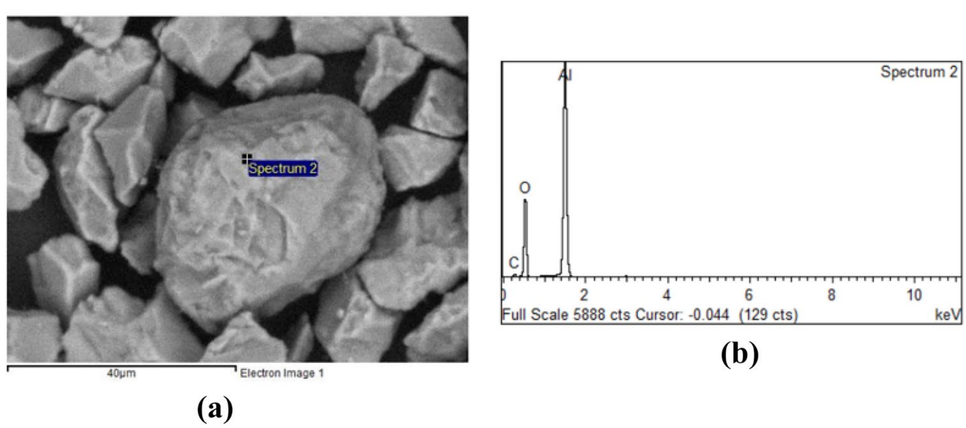

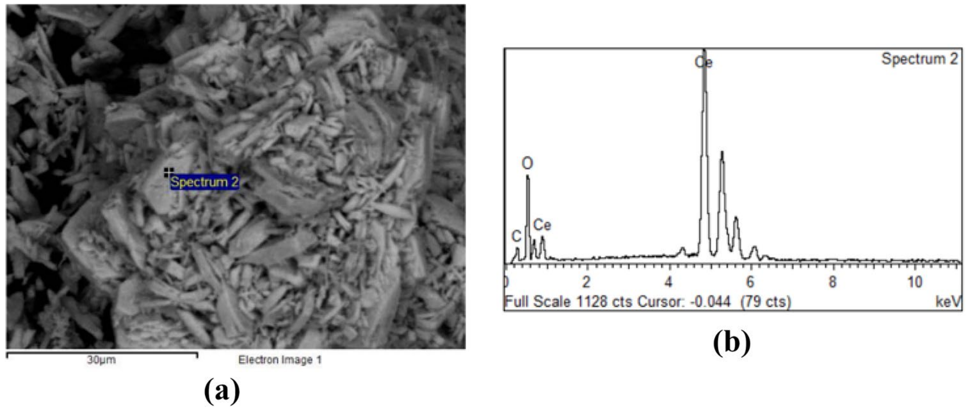


**Fig. 4** EDAX analysis of powder feedstock of $CeO_2$ (**a**) $CeO_2$ (**b**) Spectrum

**Table 5** EDAX analysis of $CeO_2$

| Element line | Weight % |
|---|---|
| O K | 24.75 |
| Ce L | 75.25 |
| Total | 100 |

**Table 6** Thickness of the coating

| Feedstock powder | Type of coat | Thickness |
|---|---|---|
| NiAl | Bond coat | 100 µm |
| NiAl + $Al_2O_3$ + $CeO_2$ | Top coat | 200 µm |

**Table 7** Process parameters related to APS

| Parameters | Values | Units |
|---|---|---|
| Flow rate of Argon gas | 24–32 | lit/min |
| Argon gas pressure | 40–68 | psi |
| Flow rate of Hydrogen gas | 6–14 | lit/mm |
| Hydrogen gas pressure | 48 | psi |
| Powder feed rate | 95–130 | gms/min |
| Standoff distance | 2–5 | inch |
| Current | 460 | Amps |
| Voltage | 50–60 | volts |

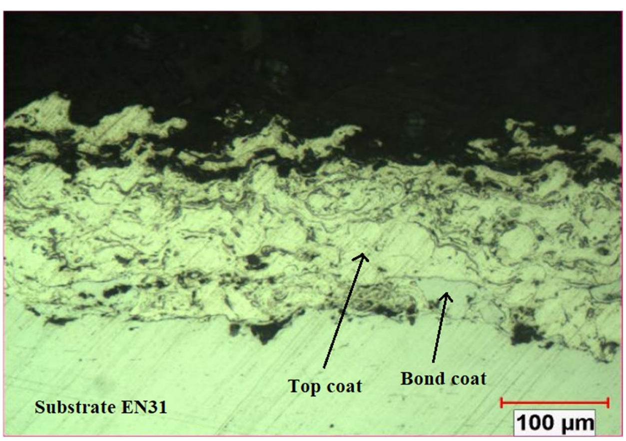


**Fig. 5** Cross sectional image of coated EN31

electrode (SCE) is used as the reference electrode. Corrosion medium consists of 3.5% NaCl solution. Potentials were measured with respect to the SCE. Test was conducted using CHI 660C model electrochemical workstation consisting of cyclic voltammetry tri-electrode chamber and electrochemical analyzer shown in Fig. 6a and Fig. 6b. Polarization curves were acquired to study the corrosion resistance of uncoated and coated bearing steel EN31 surfaces. Scanning rate 0.01 V/s was applied during the test. 30-min time duration was used for achieving equilibrium potential before conducting electrochemical measurement. Zview software was used to analyze impedance data parameters from equivalent circuit used. Value constant phase element (CPE) and charge transfer resistance (Rct) were determined by employing Nyquist plot. Salt spray test was conducted using concentration of salt solution with 5% of NaCl under temperature of 35 °C. Test coupon was subjected to salt spray for a period of 48 h under the salt spray chamber. During salt spray test, the sealed coupons were continuously exposed to the corrosion medium spray for a period of 48 h. Test coupon was suspended in vertical direction. The salt spray solution which was used as corrosion medium was near-neutral 5.0 wt% NaCl with chamber temperature maintained at 35 °C. The pH of the collected salt solution is determined.

## 2 Test Results and Discussion

### 2.1 Microstructure of Coating

Surface morphology of coated EN31 surface is investigated using SEM. Figure 7 reveals surface microstructure of coated EN31. Fig. 8 shows EDAX analysis of coating surface at Point A. SEM images reveal that the coated surface

**Fig. 6** **a** Cyclic voltammetry tri-electrode chamber **b** Electrochemical analyser

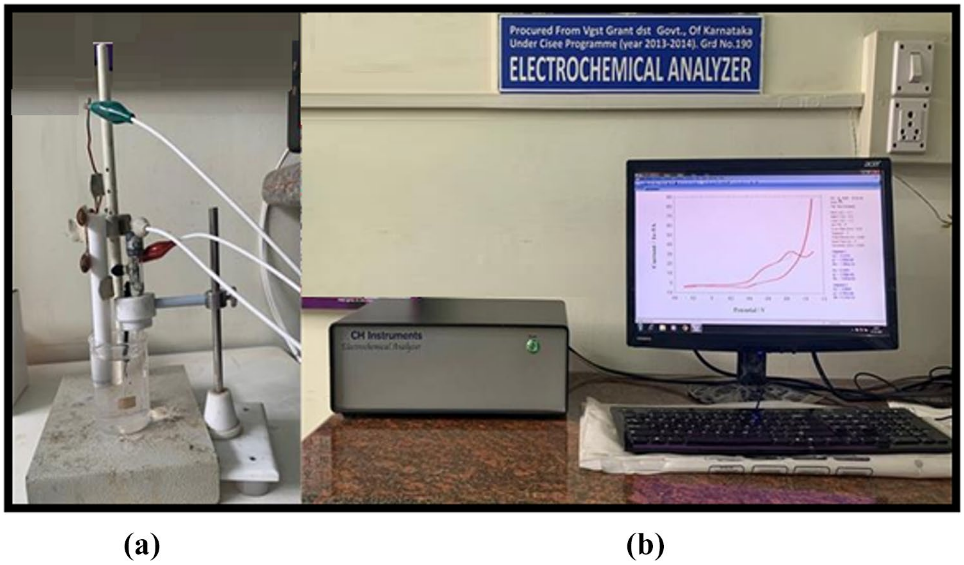


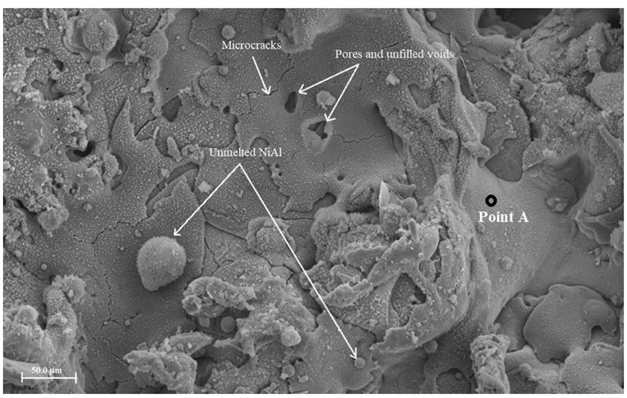


**Fig. 7** Microstructure of coated sample

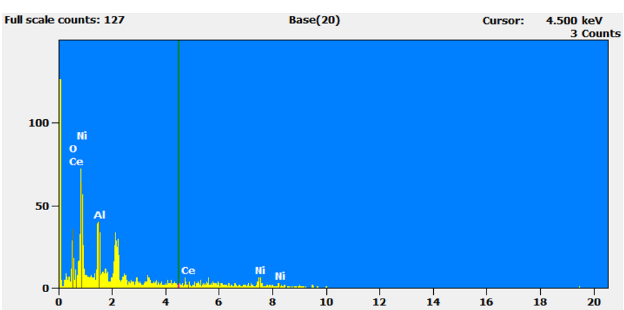


**Fig. 8** Energy spectrum analysis at Point A

is uneven, non-uniform in addition to pores on the surface. Coated surface shows existence of microcracks along with partially melted powder particles. Results from EDAX analysis show that the composite coating has different fractions of elements Ni, Al, Al, and Ce along with oxides. Maximum amount of Ni is found at Point A, whereas small quantity of Ce is also detected as indicated in Table 8. Oxides on the surface are also detected due to exposure to atmosphere.

**Table 8** EDAX analysis of composite coating

| Element line | Weight % |
|---|---|
| O K | 13.49 |
| Al K | 25.49 |
| Ni K | 50.89 |
| Ce L | 10.12 |
| Total | 100 |

Figure 9 shows XRD results of the coated sample. Phase analysis on coating surface was investigated where X-rays from XRD machine penetrated coated surface at angles between 0 and 90. XRD pattern showed numerous peaks showing the presence of different elements on coated surface. Sharp peak observed at 2 h, approximately at 45° and corresponds to Ni and Al along with oxide content. Ce element in addition to oxide content on coated surface is reflected with smaller peaks. The presence of Al element on the coating surface can also so be seen at different peaks.

## 2.2 Porosity of Coating

Porosity is a significant parameter which influences the properties of a coating. It can deteriorate the protective performances of the coatings in harsh working environments. High level of porosity in a coating can lead to high rate of corrosion [20]. Area % Porosity for $NiAl + Al_2O_3 + CeO_2$ composite coating was found to be 1.34%. Lesser porosity is due to the presence of $CeO_2$ in addition to $Al_2O_3$ in composite coating that improves crystal grains thereby reducing porosity in composite coatings [21–23].

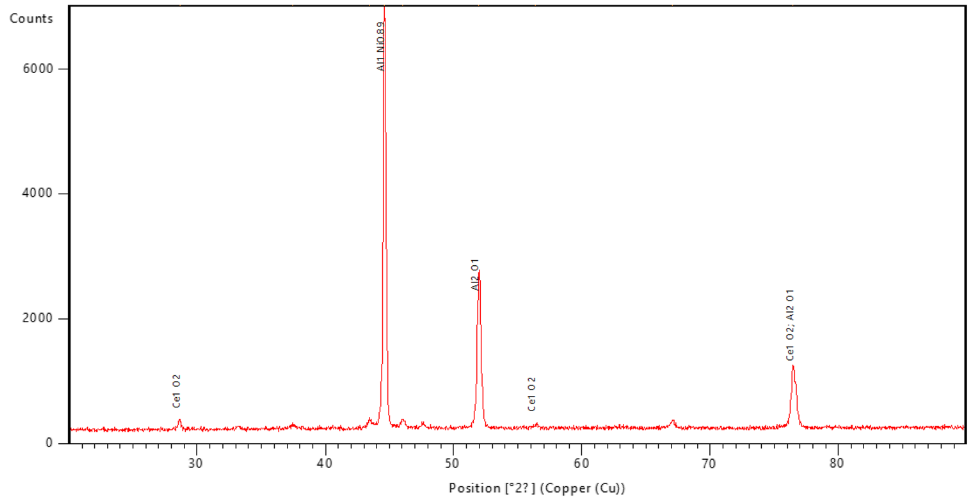


**Fig. 9** XRD of coated sample

**Table 9** Measurement of electrochemical polarization parameters for uncoated and coated EN31

| Specimen name | $E_{corr}$ (V) | $I_{corr}$ (A/cm$^2$) | Corrosion rate (gm/hr) |
|---|---|---|---|
| Uncoated EN31 | − 0.73 | − 3.7 | 6.626E-05 |
| NiAl + $Al_2O_3$ + $CeO_2$ coated EN31 | − 0.53 | − 4.4 | 1.595E-05 |

## 2.3 Polarization Test Measurement

Polarization tafel technique was employed to assess corrosion characteristic of uncoated and coated EN31. Generally, a higher value of corrosion potential ($E_{corr}$) and a lower value of corrosion current density ($I_{corr}$) indicate better corrosion protection [24]. $I_{corr}$ is obtained from the intersection of the linear portions of the anodic and cathodic curves. From the Tafel plot shown in Fig. 10, it is clear that composite coating NiAl + $Al_2O_3$ + $CeO_2$ has moved anodic and cathodic polarization curves to lower corrosion current density and toward higher corrosion potential indicating better corrosion protection on EN31. The electrochemical parameters obtained from the Tafel plots for Uncoated EN31 and Coated EN31 are summarized in Table 9. The results indicate that the NiAl + $Al_2O_3$ + $CeO_2$ coated EN31 shows higher $E_{corr}$ and lower $I_{corr}$ value than the uncoated EN31 due to coating acting as protective barrier on the surface of EN31. Coated EN31 has an $E_{corr}$ of –0.53 V which is 30% more when compared with uncoated EN31. Coated EN31 has an $I_{corr}$ of –4.4 A/cm$^2$ which is 15% less when compared with uncoated EN31.

## 2.4 Electrochemical Impedance Spectroscopy

Electrochemical Impedance Spectroscopy (EIS) like Tafel plot is an important technique used to evaluate corrosion resistance properties of coating and can also be used to predict effectiveness of coatings system [25]. EIS circuit consists of reference electrode (RE),working electrode (WE), electrolyte solution resistance ($R_s$), the charge transfer resistance ($R_{ct}$), the double layer capacitance ($C_{dl}$), warburg part (W), constant phase element ($Q_1$), and low frequency capacitance ($Q_2$). Changes in electrical properties of these circuit elements are used to study the performance of the coating. Corrosion of coated EN31 or uncoated EN31 is modeled by choosing an appropriate equivalent circuit. The impedance (Z) parameter depends on $R_{ct}$, $R_s$, electrical double layer capacitance, and AC signal frequency. In general, a larger diameter of semicircle (charge transfer resistance) means a smaller corrosion rate and Zreal indicates measure of resistance to corrosion [26]. Figure 11 shows the Nyquist plots of uncoated EN31 and coated EN31 samples. In Nyquist plot, it can be seen that the coated specimen has larger semicircle diameter when compared to uncoated EN31 indicating that the resistance to corrosion is high in coated EN31. The curve fitting on the experimental electrochemical data was fitted well and equivalent circuit fit is shown in Fig. 12.

Different parameters from EIS data for uncoated EN31 and coated EN31 are given in Table 10. Increased impedance value in the wide range of frequency for coated EN31 is indicating that coating is acting as barrier on the surface of EN31 to hinder corrosion progress. These results clearly indicate that the corrosion protection is enhanced by 27% by coating NiAl + $Al_2O_3$ + $CeO_2$ on EN31 when compared with uncoated EN31.

## 2.5 Salt Spray Test Results

Corrosion characteristic of uncoated EN31 and coated EN31 was investigated using salt spray testing in a neutral mist of 5 wt% NaCl at 35 °C for 48 h. Table 11 shows the weight loss measurements for 12, 24, 36, and 48 h for both uncoated

**Table 10** Various impedance parameters for uncoated and coated EN31

| Specimen name | $R_s$ (Ω) | $R_{ct}$ (Ω) | $R_1$ (Ω) | $C_{dl}$ (F) | $Q_1$ (rad/S) | $Q_2$ (F) | W |
|---|---|---|---|---|---|---|---|
| Uncoated EN31 | 11.91 | 224.0 | 200.2 | 6.2E-05 | 4.72E-09 | 1.66E-05 | 0.0018 |
| Coated EN31 | 0.001 | 17.14 | 254.4 | 2.8E-09 | 0.1115 | 9.03E-07 | 0.0016 |

**Table 11** Weight loss data from salt spray test for uncoated and coated EN31

| Sample Name | Salt Solution | Temperature (°C) | Exposure Time (hours) | Weight loss (g) |
|---|---|---|---|---|
| Uncoated EN31 | 5% NaCl | 35 | 48 | 0.048 |
| Coated EN31 | 5% NaCl | 35 | 48 | 0.0091 |

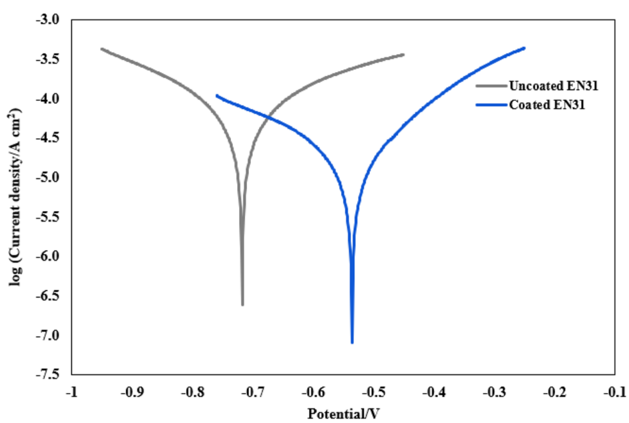


**Fig. 10** Tafel plots for Uncoated EN31 and Coated EN31

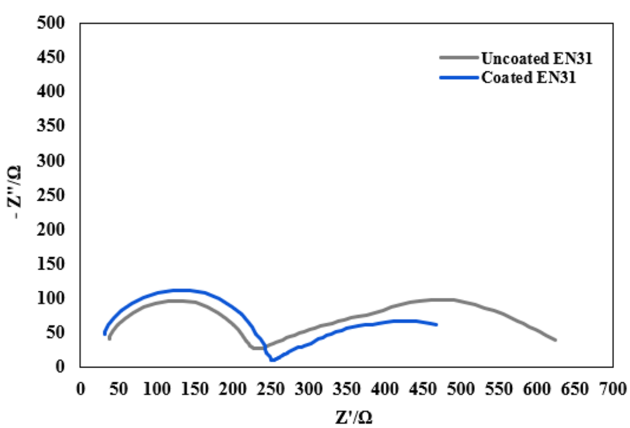


**Fig. 11** Nyquist plots for Uncoated EN31 and Coated EN31

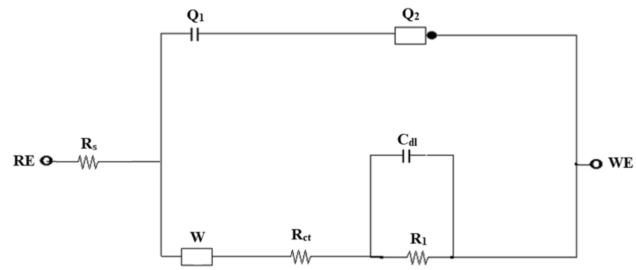


**Fig. 12** Equivalent circuit to fit EIS Data for Uncoated EN31 and Coated EN31

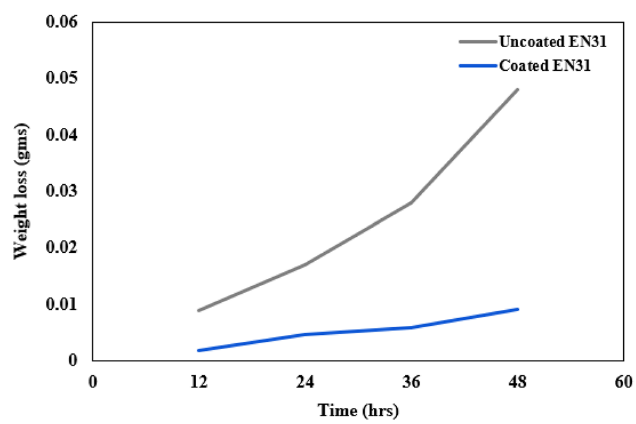


**Fig. 13** Weight loss plot from Salt Spray test for Uncoated and Coated EN31

EN31 and coated EN31 under salt spray test. Figure 13 shows high corrosion was noticed on the uncoated EN31, while there was no obvious corrosion phenomenon on the coated EN31. It was observed that red rust, non-uniform corrosion along with red dots was formed within 24 h on the surface of uncoated EN31 and weight loss was severe. Crevice corrosion was observed on the surface of uncoated EN31, whereas coated EN31 exhibited the higher corrosion resistance. Composite coating protected the surface of EN31 from severe corrosion and from material loss. Due to coating thickness and density, EN31 surface was protected from localized chemical attack of salt bath.

## 2.6 Worn Surface Morphology

Worn surface morphology of uncoated EN31 and coated EN31 post electrochemical test and salt spray test through SEM was studied. Figure 14a and b shows Uncoated and coated surface of EN31 after electrochemical test. SEM images shows that more surface is corroded for uncoated EN31. Uncoated EN31 surface directly subjected to corrosion attacks leading to pitting corrosion of the uncoated

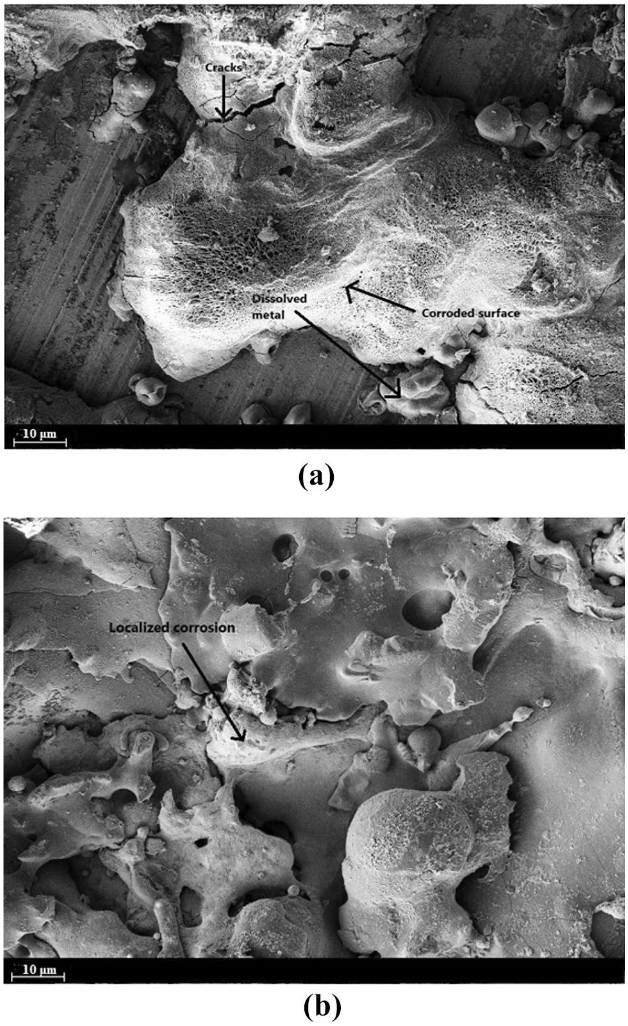


**Fig. 14** Microstructure post electrochemical test **a** Uncoated EN31;**b** Coated EN31

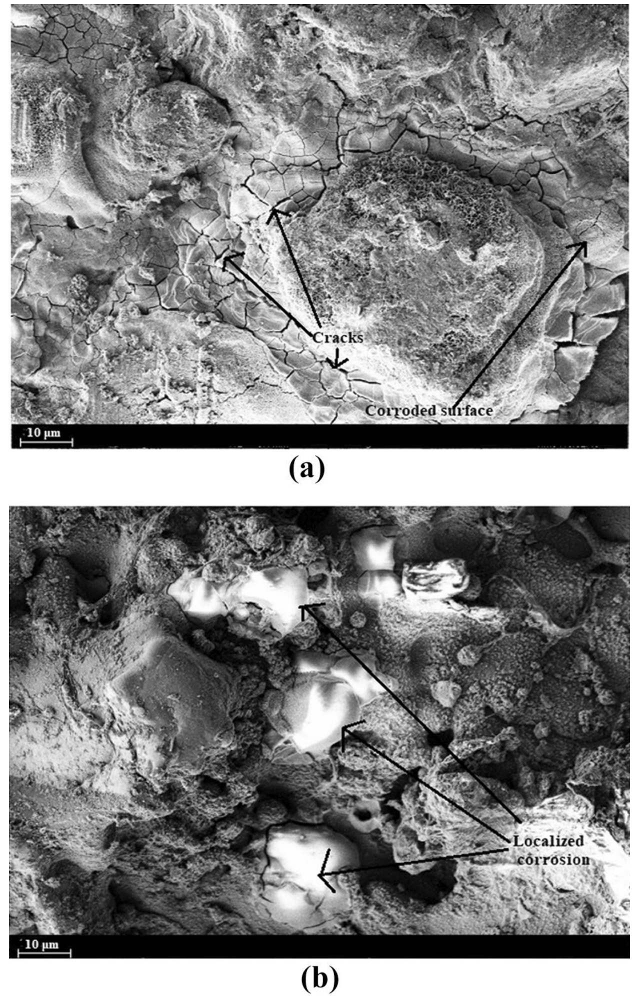


**Fig. 15** Microstructure post salt spray test **a** Uncoated EN31;**b** Coated EN31

EN31 thereby accelerating corrosion process. Figure 14b shows that the composite coating after the test has minor cracks, probably due to accelerated anodic polarization and localized corrosion on the surface. Examination of SEM images of the surface layer revealed that some of the layer of coating had microcracks and cracks extend from the coating surface up to the EN31 substrate. It can be seen from SEM images that the EN31 with composite coating is able to withstand more chemical attacks and resist corrosion process. $NiAl + Al_2O_3 + CeO_2$ coating on EN31 improves corrosion resistance.

Figure 15a and b shows Uncoated EN31 and coated EN31 after salt spray test. Chloride ion presence on the uncoated surface of EN31 introduces generalize corrosion and accelerates high corrosion rate. After 36 h pitting, corrosion was observed on the surface of uncoated EN31 resulting in material loss and further active dissolution. A clear visual changes were observed on the uncoated EN31 surface post the tests. Localized corrosion was observed on coated EN31. Corrosion probably occurred because the chloride ions penetrated either through the pores and microcracks caused by coating process or solution infiltrated between interface of the substrate/coating through defects. Detachment of the composite coating was not observed.

## 3 Conclusions

Based on the investigation performed in this study, following conclusions were drawn:

(1) Area % Porosity for $NiAl + Al_2O_3 + CeO_2$ composite coating is 1.34%
(2) Coated EN31 shows 27% higher corrosion resistance compared to uncoated EN31 under electrochemical test

(3) Coated EN31 has a corrosion potential Ecorr of − 0.53 V which is 30% more when compared with uncoated EN31
(4) Uncoated EN31 lost 5 times more weight than the coated EN31 after salt spray test
(5) Uncoated EN31 showed general corrosion and active material dissolution under both electrochemical and salt spray test
(6) Localized corrosion was observed for coated EN31 under both electrochemical and salt spray test

**Author contributions** Author MIK conducted experiments, analyzed, and interpreted experimental results and prepared draft manuscript. Author SSH designed and conceptualized experiments. Author AH contributed toward drafting manuscript. Author KR analyzed and interpreted experimental results. All authors reviewed the results and approved the final version of the manuscript.

**Funding** No funding was received for this work.

**Data Availability** The datasets generated during the current study are available from the corresponding author on reasonable request.

## Declarations

**Conflict of interest** We wish to confirm that there are no known conflicts of interest associated with this publication and there has been no significant financial support for this work that could have influenced its outcome.

## References


1. Rolling bearings – Damage and failures - Terms, characteristics and causes, ISO 15243:2004(E), 2004.
2. Xu C, Du L, Yang B, Zhang W (2011) Study on salt spray corrosion of Ni–graphite abradable coating with 80Ni20Al and 96NiCr–4Al as bonding layers. Surf Coatings Technol. https://doi.org/10.1016/j.surfcoat.2011.03.007
3. Jam A, Derakhshandeh SMR, Rajaei H, Pakseresht AH (2017) Evaluation of microstructure and electrochemical behavior of dual-layer NiCrAlY/mullite plasma sprayed coating on high silicon cast iron alloy. Ceram Int 43(16):14146–14155
4. Seong-jong KIM, Seong-kweon KIM, Jae-cheul PARK (2012) Comparison of electrochemical properties of atmospheric pressure plasma coatings for $Al_2O_3$–$3TiO_2$ and CoNiCrAlY in sea water. Trans Nonferrous Metals Soc China 22(Supplement 3):s745–s752
5. Verdian MM, Raeissi K, Salehi M (2010) Corrosion performance of HVOF and APS thermally sprayed NiTi intermetallic coatings in 3.5% NaCl solution. Corros Sci 52(3):1052–1059
6. Gao Z, Ji G, Shi Z, Wang X (2021) The tribocorrosion behaviour of YSZ coating deposited on stainless steel substrate in 3.5 wt% NaCl solution. Ceram Int. https://doi.org/10.1016/j.ceramint.2021.04.107
7. Zavareh MA, Sarhan AADM, Zavareh PA, Basirun WJ (2016) Electrochemical corrosion behavior of carbon steel pipes coated with a protective ceramic layer using plasma and HVOF thermal spray techniques for oil and gas. Ceram Int 42(2):3397–3406
8. Yangjia LIU, Xizhi FAN, Shuibing ZENG, Ying WANG, Binglin ZOU, Lijian GU, Xiaolong CHEN, Khan ZS, Daowu YANG, Xueqiang CAO (2012) Corrosion behavior of coating with plasma sprayed 8YSZ on the surface of carbon steel. J Rare Earths 30(6):592–598
9. Sathyavageeswaran SS, Manivasagam G (2016) Comparative study on corrosion behavior of plasma sprayed $Al_2O_3$, $ZrO_2$, $Al_2O_3/ZrO_2$ and $ZrO_2/Al_2O_3$ coatings. Trans Nonferrous Metals Soc China 26:1336–1344. https://doi.org/10.1016/S1003-6326(16)64236-X
10. Sreenivasa Rao KV, Girisha KG, Anjan S, Abhilash Sharma N (2017) Experimental investigation of corrosion behavior of plasma sprayed $Cr_2O_3$ coatings on 410 grade steel. Mater Today 4(9):10254–10258
11. Bijalwan P, Singh C, Kumar A, Sarkar K, Rani N, Laha T, Banerjee A, Mondal K (2021) Corrosion behaviour of plasma sprayed Fe based metallic glass (Fe73Cr2Si11B11C3 (at%) coatings in 3.5% NaCl solution. J Non Cryst Solids 567:120913
12. Kubatík TF, Lukáč F, Stoulil J, Ctibor P, Průša F, Stehlíková K (2017) Preparation and properties of plasma sprayed NiAl10 and NiAl40 coatings on AZ91 substrate. Surf Coat Technol 319:145–154
13. Guo J, Wang Z, Sheng L, Zhou L, Yuan C, Chen Z, Song Li (2012) Wear properties of NiAl based materials. Prog Nat Sci 22(5):414–425
14. Sadeghi E, Markocsan N, Nylen P (2016) A comparative study on Ni-based coatings prepared by HVAF, HVOF, and APS methods for corrosion protection applications. J Therm Spray Technol 25:1604–1616. https://doi.org/10.1007/s11666-016-0474-9
15. Praveen AS, Sarangan J, Suresh S, Siva Subramanian J (2015) Erosion wear behaviour of plasma sprayed NiCrSiB/$Al_2O_3$ composite coating. Int J Refract Metals Hard Mater 52:209–218
16. Yin Z, Tao S, Zhou X, Ding C (2008) Microstructure and mechanical properties of $Al_2O_3$–Al composite coatings deposited by plasma spraying. Appl Surf Sci 254(6):1636–1643
17. Saladi S, Menghani J, Prakash S (2015) Effect of $CeO_2$ on cyclic hot-corrosion behavior of detonation-gun sprayed $Cr_3C_2$ -NiCr coatings on Ni-based superalloy. J Mater Eng Perform 25:1379
18. Zhao X, Liu G, Zheng H, Cao H, Liu X (2015) Dose-dependent effects of $CeO_2$ on microstructure and antibacterial property of plasma-sprayed $TiO_2$ coatings for orthopedic application. J Therm Spray Technol 24:401–409
19. Mohammed Ibrahim K, Havaldar SS, Hiriyannaiah A (2021) Composition optimization for NiAl + $Al_2O_3$ + CeO composite coating on bearing steel by air plasma spray. Mater Today 46(13):6035–6040
20. Schiefler Filho MFO, Buschinelli AJA, Gärtner F, Kirsten A, Voyer J, Kreye H (2004) Influence of process parameters on the quality of thermally sprayed X46Cr13 stainless steel coatings. J Braz Soc Mech Sci Eng 26:98–106
21. He L, Tan Y, Wang X, Xu T, Hong X (2014) Microstructure and wear properties of $Al_2O_3$-$CeO_2$/Ni-base alloy composite coatings on aluminum alloys by plasma spray. Appl Surf Sci 314:760–767. https://doi.org/10.1016/j.apsusc.2014.07.047
22. Yin B, Liu G, Zhou H, Chen J, Yan F (2010) Microstructures and properties of plasma sprayed FeAl/$CeO_2$/$ZrO_2$ nano-composite coating. Appl Surf Sci 256(13):4176–4184
23. Ma W, Ge Y, Zhang L, Chen F, Zheng Y, Qi Z (2020) Study on the friction performance of cerium oxide on supersonic flame-sprayed WC-10Co-4Cr coating. Coatings 11:24. https://doi.org/10.3390/coatings11010024
24. Chang K-C, Hsu C-H, Hsin-I Lu, Ji W-F (2014) Advanced anticorrosive coatings prepared from electroactive polyimide/graphene nanocomposites with synergistic effects of redox catalytic

capability and gas barrier properties. Express Polym Lett 8:243–255. https://doi.org/10.3144/expresspolymlett.2014.28
25. Park S-M, Yoo J-S (2003) Electrochemical impedance spectroscopy for better electrochemical measurements. Anal Chem 75:455A-461A. https://doi.org/10.1021/ac0313973
26. Zucchi F, Grassi V, Frignani A (2006) Monticelli C and Trabanelli G: electrochemical behaviour of a magnesium alloy containing rare earth elements. J Appl Electrochem 36:195–204. https://doi.org/10.1007/s10800-005-9053-3